

# UC Berkeley

## UC Berkeley Previously Published Works

### Title

Upper-Tropospheric Troughs and North American Monsoon Rainfall in a Long-Term Track Dataset

### Permalink

<https://escholarship.org/uc/item/24x7f9j4>

### Journal

Journal of Geophysical Research: Atmospheres, 126(20)

### ISSN

2169-897X

### Authors

Igel, Matthew R  
Ullrich, Paul A  
Boos, William R

### Publication Date

2021-10-27

### DOI

10.1029/2021jd034541

### Copyright Information

This work is made available under the terms of a Creative Commons Attribution-NoDerivatives License, available at <https://creativecommons.org/licenses/by-nd/4.0/>

Peer reviewed

1 **Upper-tropospheric troughs and North American monsoon rainfall**  
2 **in a long-term track dataset**

3 Matthew R. Igel<sup>1</sup>, Paul A. Ullrich<sup>1,2</sup>, William R. Boos<sup>2,3</sup>

4 <sup>1</sup>Department of Land, Air and Water Resources, University of California Davis, Davis, 95616,  
5 USA

6 <sup>2</sup>Climate and Ecosystem Sciences Division, Lawrence Berkeley National Laboratory, Berkeley,  
7 94720, USA

8 <sup>3</sup>Department of Earth and Planetary Science, University of California Berkeley, Berkeley,  
9 94720, USA

10  
11 *Correspondence to:* Matthew Igel (migel@ucdavis.edu)

12  
13 **Key Points:**

- 14 • Upper-tropospheric troughs over southwest North America are identified in an  
15 atmospheric reanalysis, yielding a 40-year track dataset.
- 16 • Tropical upper-tropospheric troughs weakly but negatively affect North American  
17 Monsoon precipitation intensity in the trough center.
- 18 • When composited along the TUTT track, enhanced precipitation falls outside the main  
19 TUTT circulation.

20 **Abstract.** The North American monsoon is frequently affected by transient, propagating upper  
21 tropospheric vorticity anomalies. Sometimes called Tropical Upper-Tropospheric Troughs  
22 (TUTTs), these features have been claimed to episodically enhance monsoon rainfall. Here we  
23 track long-lived TUTTs in 40 years of reanalysis data, producing composites and case studies  
24 from 340 TUTTs which last, on average, seven days as they move westward across the North  
25 American monsoon region. TUTTs are thought to form from midlatitude Rossby wave breaking;  
26 case studies from our dataset support this theory. TUTTs move westward within the easterly  
27 upper-level flow in which they are embedded. In vortex-centered composites along the full  
28 tracks of long-lived TUTTs, we find no detectable increase in rainfall within the main TUTT  
29 circulation. Instead, negative precipitation anomalies lie within about 500 km of the TUTT  
30 center. Quasi-geostrophic ascent occurs in the southeast quadrant of TUTTs but is confined to  
31 the upper troposphere and does not appear to interact with precipitation. Positive anomalies of  
32 ascent and rainfall occur south and southeast of TUTTs but lie outside the main TUTT vortex,  
33 perhaps indicating concurrent variations in nearby climatological precipitation maxima. In  
34 contrast with previous case studies and subjective analyses that showed TUTTs enhance  
35 precipitation in parts of northwestern Mexico, our composites along the tracks of long-lived  
36 TUTTs portray these systems, to first order, as strong vorticity anomalies trapped in the upper  
37 troposphere that interact only weakly and indirectly with precipitation.

38

## 39 **1. Introduction**

40 In all monsoon climates, the region of peak seasonal mean precipitation lies on the  
41 equatorial side of an upper-level anticyclone. Mid- to upper-level vorticity anomalies that are  
42 both carried by and draw energy from this anticyclonic flow have been clearly documented in the  
43 South Asian monsoon (Hsu & Plumb, 2000; Krishnamurti & Bhalme, 1976; Ortega et al., 2017)  
44 and the North American monsoon (NAM) (Bieda et al., 2009; Newman & Johnson, 2012; Pytlak  
45 et al., 2005). These transient vorticity anomalies, in turn, interact with the background vertical  
46 shear and the moisture field in ways that have been claimed to alter regional precipitation.

47 For the North American monsoon in particular, westward-propagating upper-tropospheric  
48 disturbances are the most frequently occurring transient synoptic feature. They exist on nearly  
49 half of the days in an average summer season and are believed to contribute 20-25% of total  
50 summer precipitation in northern Mexico (Douglas & Englehart, 2007b). They are often called  
51 inverted troughs (IVs) or tropical upper-tropospheric troughs (TUTTs), named for the local  
52 minimum in geopotential that can be open to the equator and is typically most prominent  
53 between 200-500 hPa (Kelly & Mock, 1982; Newman & Johnson, 2012).

54 Despite the prevalence of TUTTs and their claimed contribution to the bulk water budget  
55 of the NAM region, many of the details of their induced precipitation patterns are unknown. For  
56 a cluster of rain gauges in northwestern Mexico, Douglas and Englehart (2007b) documented  
57 peak rainfall occurring west of the minimum 500 hPa geopotential in a 35-year climatology of  
58 IVs developed from weather maps (the west side of the TUTT would be the leading edge of the  
59 westward-propagating disturbance). In contrast, Pytlak et al. (2005) argued, based on case  
60 studies from the 2003-2004 North American Monsoon Experiment (NAME) (Higgins et al.,  
61 2006), that precipitation occurred on both the western and eastern sides of TUTTs, primarily due

62 to the organization of mesoscale convective systems (MCSs) in those regions. Whitfield and  
63 Lyons (1992) found peak precipitation in the southeast quadrant of a TUTT but did so with only  
64 one case study over Texas, which is itself well to the east of the NAM region.

65         Some of these discrepancies in the location of peak precipitation relative to the TUTT  
66 center were reconciled by Finch and Johnson (2010), who performed detailed analyses of the  
67 quasi-geostrophic (QG) motion in one TUTT that was well-observed during the NAME field  
68 campaign. They found synoptic descent to the west of that TUTT was forced by thermal  
69 advection but that, despite this QG subsidence, topographic forcing resulted in enhanced  
70 convection in that region. This picture was refined by Newman and Johnson (2012), who  
71 argued, based on constrained cloud-resolving simulations of the same 2004 case study, that the  
72 TUTT enhanced CAPE and layer shear over the Sierra Madre mountain range. These findings,  
73 which suggest TUTTs prime an environment so that mesoscale processes can produce  
74 precipitation, are distinct from the earlier suggestion by Pytlak et al. (2005) that forcing for  
75 MCSs and precipitation was synoptic.

76         While much of our understanding of TUTTs has come from case studies, especially of  
77 NAME-year features (Finch & Johnson, 2010; Newman & Johnson, 2012; Pytlak et al., 2005),  
78 there have been several systematic attempts to identify TUTTs in observational data. As  
79 mentioned above, Douglas and Englehart (2007b) produced a 35-year analysis of transients  
80 moving across northern Mexico, though this was based primarily on manual inspection of  
81 surface and 500 hPa daily weather maps and likely included a wide variety of westward-  
82 propagating mid- and lower-tropospheric features in their IV category. They suggested that  
83 precipitation was enhanced to the east and west of the TUTT center. An empirical orthogonal  
84 function analysis of NAM synoptic variability in eight years of satellite-derived precipitation and

85 reanalysis data showed that QG lifting around TUTTs plays a negligible role in organizing  
86 precipitation, with TUTT-induced vertical shears causing MCSs to form northwest of the TUTT  
87 center (Seastrand et al. 2015). Bieda et al. (2009) identified TUTTs from 1980-2002 in the  
88 North American Regional Reanalysis (NARR), finding an enhancement of total moisture in the  
89 NAME region and an enhancement of the amplitude of the diurnal cycle of lightning activity on  
90 days with TUTTs. Lahmers et al. (2016) found a long-term (1951-2010) increase in northern  
91 NAM TUTT track density in downscaled WRF simulations forced with the NCEP-NCAR  
92 reanalysis (Kalnay et al., 1996). Luong et al. (2017) found a long-term increase in atmospheric  
93 moisture and convective instability in simulations of historical severe weather events during the TUTT  
94 season. Together, these studies suggest a weak but consistent enhancement of regional  
95 precipitation from TUTTs in northwestern Mexico.

96         Additionally, some studies have pointed to important indirect effects of TUTTs on  
97 precipitation in the NAM. Rogers and Johnson (2007) and Johnson et al. (2007) suggested that  
98 TUTTs may be important contributors to the initiation of moisture surges in the Gulf of  
99 California, from which further circulations and convection may later develop.

100         The goal of this study is to create a dataset of time-resolved North American monsoon  
101 TUTT tracks (not just maps of climatological track density) in multiple decades of a modern  
102 reanalysis, then to use those tracks to improve understanding of TUTT structure and  
103 precipitation. One of our most rudimentary objectives is to validate the summary by Newman  
104 and Johnson (2012) that NAM TUTTs "are unique because they have enhanced precipitation on  
105 the western side ... while TUTTs throughout the rest of the world typically have enhanced  
106 precipitation on the eastern flank." In fact, we will show that this statement is not generally true  
107 along the entire track of long-lived TUTTs in the Central American domain, and the 2004 case  
108 studies that dominated such thinking may be anomalies in the longer climatology of NAM

109 TUTTs, unless the ERA5 reanalysis used here is somehow anomalous in its representation of the  
110 2004 monsoon season. On a more detailed level, we seek to understand the mechanisms by  
111 which a TUTT alters precipitation, reconciling, if possible, the arguments by several prior studies  
112 that QG lifting is important (Pytlak et al. 2005) with those that find it is negligible in magnitude  
113 and thus insignificant compared to the effect TUTTs have on MCS formation through their  
114 influence on the environmental vertical shear (Newman and Johnson 2012, Seastrand et al.  
115 2015). Our methodology contrasts strongly with that of prior work that has focused on case  
116 studies of small numbers of TUTTs over particular regions of Mexico (Pytlak et al. 2005,  
117 Newman and Johnson 2012) or that has used subjective identification of troughs based on criteria  
118 that include a variety of middle- and lower-tropospheric disturbances (Douglas and Englehart  
119 2007). We seek to paint a picture of strong, long-lived NAM TUTTs along the entire length of  
120 their track.

121 This paper is organized as follows. First, we detail our methodology for identification  
122 and tracking of TUTTs. Our catalogue of TUTTs then enables us to describe their genesis and  
123 meteorology, their properties beginning with their dry dynamics, their moisture structure, and  
124 finally their associated mechanisms for precipitation production. These results are then  
125 summarized together with conclusions.

## 126 **2. Identification and Tracking**

127 We used TempestExtremes (Ullrich et al., 2021; Ullrich & Zarzycki, 2017) to track  
128 TUTTs. TempestExtremes is a flexible software package for identifying and tracking  
129 meteorological features in time and space in historical or simulated datasets. We used three  
130 search criteria to track TUTTs – 1) a 200 hPa stream function-indicated cyclonic rotation center  
131 (i.e. local minimum) with 2) no greater than a 325 m rise from the center over  $1^\circ$  in the 1000 hPa

132 height field and 3) selection of only the strongest local minima within  $5^\circ$  great circle distance  
133 (see §6). The first criterion helped us locate rotational upper-tropospheric disturbances at a level  
134 where they are considered to be the strongest (Kelly & Mock, 1982). The second criterion was  
135 added to prevent surface-based meteorological phenomena (e.g. tropical cyclones) from entering  
136 the dataset. We estimated appropriate parameter values for the second criterion from Zarzycki  
137 and Ullrich (2017). These criteria were applied to 40 years of hourly ERA5 (Hersbach et al.,  
138 2020) reanalysis (1979 to 2018) at  $0.25^\circ \times 0.25^\circ$  spacing. The criteria were designed to be  
139 general and applicable to other reanalyses or forecast datasets at high enough resolution to  
140 resolve synoptic-scale features like TUTTs. We tracked upper-tropospheric cyclonic  
141 disturbances between  $15^\circ\text{N}$  to  $40^\circ\text{N}$  and  $90^\circ\text{W}$  to  $120^\circ\text{W}$  (visible area in Fig. 1 and highlighted  
142 in Fig. 3). July and August are the months of peak rainfall in the NAM (Adams & Comrie,  
143 1997) and in potential vorticity (PV) streamer activity in the North Atlantic (Papin et al., 2020).  
144 So, we chose to only track entities that have at least some period of their track in July or August  
145 but which may originate or dissipate outside those months. We require that tracked disturbances  
146 last at least 2.75 days (see below) to be considered long-lived.

147         These tracking criteria result in 340 upper tropospheric disturbances which we will call  
148 TUTTs. They last up to 261 hours (see Fig. 2 next section) and 92% track from east to west  
149 across the domain. TUTT genesis does not occur preferentially at any time of day (not shown)  
150 which is consistent with a synoptic feature rather than one driven by diurnally forced convection.  
151 Figure 1a shows the number of hours with a TUTT track center in each  $0.25^\circ \times 0.25^\circ$  box (i.e.  
152 track density) over the 40 years of ERA5. Most TUTT centers occur east of the Sierra Madre  
153 Occidental and south of  $30^\circ\text{N}$ . There is a secondary maximum of occurrence over and to the  
154 west of the southern tip of the Baja California peninsula. Figure 1b provides a sense of the



155 motion of TUTTs for locations with at least 50 TUTT centers. Motion is broadly toward the  
156 west and northwest at  $\sim 5 \text{ m s}^{-1}$  with some local geographic influences to the pattern.

157         As a way of assessing our tracking method, we compare our TUTTs with those  
158 subjectively identified during the NAME year by Pytlak et al. (2005). Table 1 lists the dates of  
159 these TUTTs, including the numbered labels from Pytlak et al. (2005). We identify fewer  
160 TUTTs than Pytlak et al. (2005), but our TUTTs correspond well to disturbances they identify.  
161 Our identification method is intentionally strict since we are concerned with understanding  
162 TUTT behavior rather than quantifying all their possible impacts. Table 1 suggests a  
163 consequence of that choice is that we only identify a subset of all possible TUTTs but that we  
164 have a low false positive rate (only 1 potential false positive in the NAME year). It is possible  
165 that some of the TUTTs identified by Pytlak et al. (2005) do not pass the minimum time  
166 requirement to be included in our dataset. Our minimum longevity of 2.75 days was originally  
167 chosen because the TUTTs hand-selected by Pytlak et al. (2005) all spanned at least three days,  
168 but minimum longevities of slightly longer than 2 days or slightly shorter than 3 days would also  
169 be consistent. Regardless, TempestExtremes does a good job strictly identifying and tracking  
170 TUTTs.

171         In search of all the hand-analyzed TUTTs in Table 1, we also tested the capabilities of  
172 TempestExtremes by relaxing our search criteria to merge circulation centers within only  $3^\circ$   
173 (rather than  $5^\circ$ ) and by imposing a minimum longevity of either 0.75 days or 1.75 days. The  
174 resulting permissive TUTT dataset employing the shortest time limit includes 1373 feature tracks  
175 (quadruple our control count) across the 40 years of ERA5 data with some features on each of  
176 the days in Table 1 (“Permissive” column) as well as 23 other feature tracks in the NAME year.  
177 But the median feature longevity is just 36 hours and the dataset averages one identified TUTT

178 on nearly every day within the search domain over the 40 July-August periods. Additionally, at  
179 152 different times, there are as many as four features tracked simultaneously in our relatively  
180 small search domain. For comparison, the TUTT control dataset we use never includes more  
181 than one feature at a time. The 1.75-day limit yields 607 possible TUTTs (70% more than our  
182 control count) with a median longevity of 72 hours and up to three features tracked  
183 simultaneously. This dataset captures one more numbered TUTT in Table 1 than the control  
184 dataset, but that TUTT (number 6) is split into three features, and there are additionally five  
185 potential false positives. Such properties make these permissive datasets more inclusive of  
186 possible TUTTs (a desirable feature) but also more inclusive of possible spurious transient  
187 features (not in keeping with our goals). So, we proceed with using our strictest track dataset  
188 and note that our results should be considered in light of these relatively strict criteria.

189 Table 1 also includes hand-analyzed TUTTs that resulted in heavy precipitation events in  
190 the Lake Mead basin (Sierks et al., 2020) which is in the northwest corner of our search domain.  
191 Our dataset contains five of their eight identified TUTTs. Again, given our strict criteria this is  
192 an encouraging success rate. Sierks et al. (2020) examined 40 intense rainfall events in the Lake  
193 Mead basin in the past 40 years. Of those, 9 were related in some way to a tropical cyclone.  
194 These would not be expected to be associated with TUTTs, and indeed, our dataset does not  
195 include any of these dates. This helps confirm the contrapositive that TempestExtremes does not  
196 include tropical cyclone-associated events in the TUTT dataset.

### 197 **3. TUTT Behavior and Properties**

198 Figure 2 shows basic statistics of TUTTs for each year in ERA5. There is a remarkable  
199 long-term consistency in the number of tracked TUTTs per year (Fig. 2a). The median number  
200 of TUTTs per year is 8 with a standard deviation of just 2. Figure 2b shows the statistics of

201 TUTT longevity broken down by year. Longevity is more disperse than number and there is a  
202 weak increase of about 11 hours between 1979 and 2018 (~3% per decade). Given the  
203 possibility for this long-term trend to be influenced by changes in the observing network that  
204 provides input to the ERA5 reanalysis, we do not investigate it further here. Overall, the trends  
205 we observe are weaker than those of Douglas and Englehart (2007a) who show an increase in  
206 total inverted trough counts between 1976 and 2001 of about 14% per decade although it remains  
207 possible theirs was mostly driven by drought in the 1970s. A limitation of our statistics on  
208 TUTT lifetime is that we set an eastern boundary on the domain in which TUTTs are identified,  
209 which means some vorticity anomalies that originate east of our search domain are only counted  
210 as TUTTs after being advected into that domain (see Fig. S5a).

### 211 *3.1 Genesis*

212 To begin to investigate the physics of TUTTs, we examine the meteorology of North  
213 America before and during TUTT formation. As an example, we show 200 hPa PV (which is  
214 not used directly as a tracking variable in our application of TempestExtremes) and track center  
215 from our dataset for the TUTT previously described by Finch and Johnson (2010) and Newman  
216 and Johnson (2012) (#4 in Table 1). TempestExtremes identifies a TUTT beginning late on July  
217 8<sup>th</sup> which survives until July 14<sup>th</sup>. In Figure 3, we show PV beginning on the 7<sup>th</sup> at 12Z for  
218 meteorological context prior to TUTT genesis. All panels include the PV in colored contours  
219 and a red dashed line which marks the northernmost switch in the plotted domain from westerlies  
220 to easterlies at 200 hPa. Additionally, latter panels include a pink star marking the location of  
221 the TUTT center for the indicated day at 12Z. From July 7<sup>th</sup> through the 9<sup>th</sup>, a deep extratropical  
222 trough over the central US breaks (Haynes & McIntyre, 1987) and some of the high PV becomes  
223 embedded within the lower latitude easterlies. The TUTT center identified on July 9<sup>th</sup> is clearly

224 associated with anomalous PV over the Mississippi river and Gulf of Mexico. The TUTT center  
225 maintains its clear link to this PV source through (at least) July 12<sup>th</sup>. The TUTT moves  
226 westward slowly. Starting on the 9<sup>th</sup>, it becomes embedded in a region of weak upper-level  
227 easterlies. While we will show later that TUTTs are nearly round in a composite sense (Fig. 4),  
228 the PV associated with TUTT 4 is irregularly shaped and variable over the lifetime of the feature.

229         This kind of midlatitude-turned-subtropical PV feature has been discussed in detail in the  
230 context of events in South Asia by Ortega et al. (2017). They describe a “quasi-biweekly”  
231 process by which midlatitude Rossby waves break as they move off the east coast of Asia into  
232 the Pacific, a preferred region for Rossby wave breaking (Abatzoglou & Magnusdottir, 2006;  
233 Homeyer & Bowman, 2013). These events inject cyclonic energy into the subtropical easterlies  
234 and are hypothesized to eventually enhance precipitation in the Indian monsoon (Ortega et al.,  
235 2017). Potentially leading to a similar situation in the western hemisphere, summertime Rossby  
236 wave breaking and associated PV streamers are also common over North America and the  
237 western Atlantic (Homeyer & Bowman, 2013; Papin et al., 2020). Bosart et al. (2011) linked  
238 subsynoptic-scale PV disturbances to mesoscale convection in the NAM. Sierks et al. (2020)  
239 linked wave breaking directly to enhanced precipitation in the NAM, and Pytlak et al. (2005)  
240 noted westerly energy wrapping into the easterlies in association with TUTTs. To get a sense for  
241 how common this development sequence may be for TUTTs over North America, we have  
242 included an assessment of whether midlatitude wave breaking is associated with TUTT genesis  
243 for the disturbances listed in Table 1. Map sequences like that in Fig. 3 are included for each  
244 identified 2004 TUTT as Supporting Information. While we cannot say that TUTTs are *caused*  
245 by breaking, for three of the five NAME-year TUTTs, genesis is obviously *related* to midlatitude  
246 wave breaking near the latitude separating easterlies and westerlies. TUTT 7a/b (Fig. S3) and  $\alpha$

247 (Fig. S4) are similar in that there is wave breaking into the subtropics coincident with TUTT  
248 genesis, but in both cases, the breaking is well to the east of our search domain. For 7a/b and  $\alpha$ ,  
249 we deem wave breaking to be plausibly associated with TUTT genesis, but the direct link is not  
250 clear from the Figs. S3 and S4 alone. In all cases for the year 2004, TUTT centers are located  
251 south of the transition to easterlies despite frequently occurring at latitudes where westerlies are  
252 common. In most cases, including for TUTT 4 shown in Fig. 3, the meteorology of the CONUS  
253 is dominated by troughing on the east and west coasts with ridging (an enhanced monsoon ridge)  
254 two days prior to TUTT genesis. This pattern can be clearly seen in Fig. 3 for TUTT 4 as well  
255 as in a mean sense in the 200 hPa geopotential patterns two days prior to genesis (Fig. S5), and  
256 suggests that anticyclonic flow around the upper-level monsoon high advects vorticity anomalies  
257 into the NAM domain. Although the anomaly of the geopotential pattern prior to genesis is  
258 weak, it does suggest the upper-level pattern is amplified relative to climatology between the  
259 eastern Pacific and the peak of the monsoon ridge. Finally, while Ortega et al. (2017) observe a  
260 10-20 day cycle in events in south Asia, mean and median TUTT genesis periods for events in  
261 the same year in our data are  $\sim 7$  days and  $\sim 6$  days.

### 262 *3.2 Dynamics*

263 Above, we largely examined the properties of *individual* TUTTs. But one of the benefits  
264 of tracking TUTTs (and one of our goals in so doing) is that we can easily examine their  
265 *composite* properties. Composites are constructed about the center of identified TUTTs (i.e.  
266 approximately about minima in 200 hPa stream function). We composite data from all times  
267 with an identified TUTT equally rather than compositing by per-TUTT means. This choice  
268 allows TUTT composites to be mechanistically linked as it retains relatable magnitudes among  
269 composites. But, it has the potential to weight the composite properties to particularly strong

270 and/or long-lived events. Figure 4 shows the composite mean PV structure of TUTTs at 200 hPa  
271 and 500 hPa, giving a sense for the size and intensity of TUTTs. The composite TUTT reaches a  
272 peak intensity of  $\sim 3$  PVU at 200 hPa and exhibits a slight southwest-to-northeast tilt. At 500  
273 hPa, TUTTs only weakly influence the PV field. As their name would imply, Fig. 4 confirms  
274 TUTTs are largely upper tropospheric features; this might seem unsurprising given our choice to  
275 track 200 hPa streamfunction anomalies, but Boos et al. (2015) found peak PV at 500 hPa for  
276 disturbances identified by tracking 850 hPa relative vorticity anomalies in the South Asian  
277 monsoon. Figure 4 also shows the bulk shear of the composite wind field between two pairs of  
278 levels. The lower layer shear (850 hPa to 500 hPa) maximizes on the northwestern side of  
279 TUTTs whereas the upper layer shear (500 hPa to 200 hPa) maximizes on the southern side and  
280 minimizes near the center of the vortex. As indicated by the composites of vertical shear,  
281 rotational flow around the TUTT center extends radially outward to about  $8^\circ$  great circle  
282 distance, suggesting that any precipitation anomalies caused by this shear or by quasi-  
283 geostrophic uplift within the TUTT should be located within that radius (this will be discussed in  
284 detail in following subsections).

285         In the simplest sense, TUTT motion appears to be due to advection of the upper-level  
286 vortex by the horizontal wind. Figure 5 shows TUTT-mean horizontal wind at 500 hPa and 100  
287 hPa. While these levels bracket that of the peak intensity of the rotational flow at 200 hPa, Fig. 5  
288 clearly shows that easterlies dominate across much of the domain and especially near the TUTT  
289 center. Thus, TUTTs appear to be advected over the NAM region by the background flow from  
290 their source region east of the Rockies, though comparison of Fig. 1b to Fig. 5 suggests TUTTs  
291 move more slowly than the background wind above and below their center of peak vorticity.

292 Data in Fig. 5 is overlain on a map centered on the mean location of TUTT centers, for a sense of  
293 scale.

294 Next, we examine the vertical structure of TUTTs with composite vertical cross sections  
295 (Fig. 6). Figure 6a shows the composite mean vorticity structure of TUTTs averaged  
296 meridionally within 5 degrees latitude of the composite mean center. Figure 6b shows a similar  
297 zonal mean latitude-height composite. It should be noted that in the height profiles we present  
298 (Fig. 6, 7c, and 8), some of the input data to our composites from some TUTT times and  
299 locations may be below ground and extrapolated in the reanalysis. The mean surface pressure  
300 across all TUTTs at the TUTT center is 950 hPa. Consequently, the lowest levels in height  
301 profiles should be interpreted cautiously. The intensity of TUTT vorticity peaks at 200 hPa  
302 (which is also the level at which we identify cyclonic features from the stream function) and is  
303 weak below 500hPa, if it exists at all there. The composite TUTT is embedded within a region  
304 of anticyclonic circulation, consistent with the view that TUTTs are isolated cyclonic  
305 circulations generally moving westward in a deep monsoon anticyclone.

306 To create meaningful composites of some physical quantities, we added a new capability  
307 to TempestExtremes. The climatological patterns of vertical velocity and precipitation are  
308 highly dependent on local geography over North America and on the general circulation of the  
309 atmosphere across the tropics. For example, higher rainfall amounts occur climatologically  
310 during July and August near the southern edge of our search domain over ocean, and locally over  
311 high terrain. To prevent these climatological background signals from imprinting themselves on  
312 composites of TUTT properties, we construct composites of anomaly fields. The anomaly is  
313 here defined as the instantaneous field measure minus the long-term background state, which is  
314 composed of the first four intra-annual Fourier modes of the daily climatological mean. The first

315 four modes are kept because they recreate the NAM seasonal cycle of precipitation well but  
316 eliminate large short-term fluctuations that exist in the mean calculated from 16 years of TRMM  
317 data (see §4 below).

318 Figure 6a includes the composite of meridional mean anomalous vertical pressure  
319 velocity. In the upper troposphere below 200 hPa, TUTTs exhibit a zonal dipole of ascent, with  
320 subsidence to the west and ascent to the east of the circulation center. In the middle to lower  
321 troposphere, weak subsidence occurs at the circulation center while modest ascent peaks about  
322 1000 km to the east. This structure is in keeping with TUTTs studied in the north Pacific (Kelley  
323 & Mock, 1982; Whitfield & Lyons, 1992). TUTTs exist in a region in which the climatological  
324 shear of the zonal wind is eastward below 200hPa and westward above. Therefore, the  
325 anomalous vertical velocity expected in QG flow around a vortex changes sign at 200 hPa,  
326 consistent with the quadrupole in anomalous vertical velocity seen in the upper troposphere in  
327 Fig. 6a. Along the meridional cross section (Fig. 6b), zonal mean vertical velocity is strongly  
328 upward to the south of the vortex center and downward below the center and to the north (note  
329 the change in color scale between Figs. 6a and 6b). The strongest upward motion is located in  
330 the lower troposphere about 15° of latitude south of the TUTT center, and is likely associated  
331 with the East Pacific ITCZ (compare with the average TUTT position shown in Fig. 5, which  
332 would place that peak ascent south of Central America near 10°N). Taken together, these figures  
333 imply a region of strong anomalous upward motion near the climatological ITCZ, with the  
334 periphery of that anomalous ascent extending into the southern part of TUTTs and wrapping  
335 around to the east as one ascends from the surface to 200hPa.

336 We have also examined the dynamics responsible for the vertical motion distribution  
337 shown in Figure 6 using the traditional form of the QG  $\omega$  equation. Specifically, we inverted the



338 adiabatic terms representing differential geostrophic absolute vorticity advection and the  
339 horizontal Laplacian of horizontal geostrophic thickness advection, applied to the composite  
340 wind and thermodynamic fields. To faithfully compare composite anomalous  $\omega$  to that derived  
341 from QG, Fig. 7a shows anomalous  $\omega$  at 250 hPa minus the domain mean anomalous  $\omega$ . This is  
342 a necessary complication given the composite nature of our input. The pattern thus produced  
343 shows primary uplift in the southeast quadrant of the TUTT and subsidence immediately to the  
344 northwest, with maxima within a few hundred kilometers of the TUTT center. Figure 7b shows  
345 the same map derived from inverting the QG omega equation. The pattern and magnitude of the  
346 pressure velocity are similar. This implies that the upper-level ascent and descent in the vicinity  
347 of a TUTT center is largely the result of dry adiabatic processes rather than some interaction with  
348 moist convection, a notable finding given the great importance of diabatic effects for ascent in  
349 lower-tropospheric vortices in some monsoon regions (e.g. Murthy and Boos 2019). Figure 7c  
350 shows vertical profiles of pressure velocity. The solid lines show profiles of pressure velocity  
351 for a square region  $5^\circ$  on a side located to the southeast of the composite center minus the  
352 respective domain mean (i.e. what is shown in the previous panels). The dashed lines show the  
353 respective domain mean profiles. There is a deep layer of uplift to the southeast of the TUTT  
354 center that peaks near 250 hPa. This layer lies between two layers of descent. The QG analysis  
355 does a good job approximating the shape and magnitude of the composite anomalous  $\omega$  in these  
356 layers. This implies that the upper-level dynamics of TUTTs can be reasonably well understood  
357 with QG kinematics. However, the QG inversion fails to recreate the anomalous descent seen  
358 between the surface and 500 hPa in the composite; diabatic processes, such as friction with the  
359 high topography in the NAM region, may be important there.

360 The domain mean composite anomalous  $\omega$  (dashed red line in Fig. 7c) is dominated by  
361 the strong ascent 1000-1500 km south of the TUTT center (Fig. 6b). This raises an important  
362 question about TUTTs. Do TUTTs somehow cause anomalous ascent in the East Pacific ITCZ,  
363 or do their genesis, propagation, and sustenance occur in response to the intensification of the  
364 ITCZ? Alternatively, are the ITCZ and TUTTs both modulated by some larger-scale event, such  
365 as the wave breaking portrayed in Fig. 3? Answering this question is beyond the scope of this  
366 investigation.

### 367 *3.3 Moisture*

368 Figure 8 shows composite cross sections of the relative humidity of TUTTs. The west-  
369 to-east cross section in Fig. 8a shows the lowest values of boundary layer humidity lie on the  
370 western side of the TUTT; boundary layer-to-midlevel humidity is lesser there, as is humidity  
371 within TUTT cores above 500 hPa. In the wake of TUTTs to the east, the composite shows  
372 higher upper-level humidity than to the west. The north-to-south cross section exhibits a  
373 meridional gradient (consistent with climatology) at most levels. Together, these suggest TUTTs  
374 are the moistest to their south and east but that they are not particularly moist systems. In their  
375 cores, they are, in fact, rather dry for systems which have been claimed to cause precipitation  
376 enhancement. The water vapor scale height within the TUTT core is about 50 m lower than  
377 outside the TUTT core (not shown directly). So, TUTT cores are slightly less moist and their  
378 moisture is concentrated at lower altitudes. This combination would tend to suppress growth of  
379 deep convection within TUTT cores relative to TUTT edges.

380 Figure 9 shows the composite mean anomalous 850 hPa wind overlain on the composite  
381 mean 850 hPa water vapor mixing ratio. This figure is designed to illustrate the association of  
382 TUTTs with anomalous horizontal moisture advection and low-level convergence. There is a

383 clear enhancement of near-surface anticyclonic circulation to the northeast of the TUTT center.  
384 Given the composite center location is in central Mexico, this might be related to a strengthening  
385 of the North American low-level jet, though it is unclear why this would be associated with  
386 TUTTs. There is an anomalous convergence line at about  $-10^\circ$  likely associated with a shift or  
387 strengthening of the ITCZ. Figure 9 shows there is dry advection to the northwest of TUTTs and  
388 within the western half of the TUTT itself; mixing ratios are also larger to the east of the TUTT  
389 than to the west, likely due to the TUTT's mean location just west of the Gulf of Mexico (e.g.  
390 Fig. 5). *A priori*, it was not obvious whether TUTTs would affect moisture advection  
391 significantly since TUTTs are inherently upper tropospheric features with low boundary layer  
392 relative humidity (Fig. 8). TUTT cores mostly experience near neutral low-level moisture  
393 advection, and there is no indication that TUTTs produce any cyclonic stirring across the  
394 climatological mean moisture gradient.

#### 395 **4. TUTTs and Precipitation**

396 As discussed in the Introduction, previous studies have suggested that TUTTs may be felt  
397 most strongly in the arid NAM region through their impact on precipitation. Figure 10 shows the  
398 TUTT-mean anomalous TRMM precipitation rate where, as above, anomalies are calculated as  
399 deviations from a daily mean which retains the first four Fourier modes calculated from 1998 to  
400 2013. We use 3-hourly TRMM precipitation estimates at  $0.25^\circ$  (3B42 version 7)(Huffman et al.,  
401 2007). Figure 10 has been masked for statistical significance by comparing the statistics of the  
402 distribution of rainfall rates for TUTT cases against a climatology. Filled contours show the  
403 mean anomalous precipitation rate for TUTT rainfall distributions which pass a two-sided *t*-test  
404 at the 90% level against the climatology. The climatology is constructed by randomizing the  
405 year but not the date of TUTTs and re-compositing. In this way, we ensure that the climatology

406 contains the same number of samples from the same geographic locations with the same  
407 potential for autoregression in the data as the TUTT dataset. Approximately half of all points are  
408 deemed statistically significant by this strict test.

409         The most coherent signal to emerge from the data is that of a decrease in the magnitude  
410 of precipitation within the TUTT and to its north and northeast; the peak reduction in rainfall is  
411 centered on the west side of the TUTT, in the region where the anomalous low-level winds  
412 would be expected advection in dry air, given the total moisture gradient (Fig. 9). There are also  
413 several small contiguous regions of precipitation enhancement east, south, and west of the TUTT  
414 center.

415         The decrease in precipitation within the TUTT core is associated with the subsidence  
416 (Fig. 6) that occurs at most levels north of the TUTT center and at the mid- to low-levels in the  
417 TUTT center. It is unclear whether the subsidence anomaly is causing the precipitation anomaly,  
418 or vice-versa, a common issue in low-latitude atmospheric dynamics. Moreover, we identify no  
419 clear cause of either of these anomalies in the TUTT center. While some low-level positive  
420 moisture advection occurs north of TUTT cores (Fig. 9), it does not effect an enhancement of  
421 precipitation. One way to untangle this ambiguity in the future would be to examine TUTTs in  
422 large-domain, convection-permitting simulations (Luong et al., 2017; Prein et al., 2015).

423         There are, however, several regions of precipitation enhancement to the south of TUTTs.  
424 These contiguous regions of precipitation enhancement occur in a region of anomalous ascent (in  
425 a composite sense; Fig. 6), higher humidity (Fig. 8), neutral to anticyclonic rotation (Fig. 6), and  
426 largely in regions of weak upper tropospheric shear (Fig. 4d). They also seem to occur in  
427 regions of anomalous 850 hPa convergence but not necessarily in regions of positive moisture  
428 advection (Fig. 9). We will note two possible explanations for precipitation enhancement. First,

429 because the composite central location of TUTTs lies over central Mexico, the southern and  
430 eastern sides of TUTTs are coincident with steep topography and on-shore flow. This  
431 combination may act to enhance precipitation locally through upslope flow or frictional  
432 convergence, and the on-shore flow may be associated with the larger-scale easterlies within  
433 which the TUTT is embedded rather than the rotational flow of the TUTT itself. Second, the  
434 anomalous convergence well to the south of TUTTs may correspond to an enhanced or displaced  
435 ITCZ. The ITCZ modulation might be caused by the same wave-breaking activity that generated  
436 the TUTT, but how and why the ITCZ and TUTTs interact is unknown.

437         It is possible that TUTTs influence precipitation in geographically specific ways that vary  
438 along their full tracks. For example, case studies of TUTTs (e.g. Pytlak et al. 2005; Newman and  
439 Johnson 2012; Finch and Johnson 2010) often illustrate the scattered nature of convection  
440 associated with TUTTs in northwestern Mexico. This is in keeping with our synthesis which  
441 shows mixed impacts and only that the composite *mean* precipitation rate is lower within TUTT  
442 centers, not that high rain rates never occur in TUTTs. The upper-tropospheric nature of TUTTs  
443 seems to limit their ability to directly enhance precipitation; they produce ascent over a deep  
444 layer of the upper troposphere in their southeastern quadrant, with that ascent well-represented  
445 by quasi-geostrophic solutions unmodified by diabatic heating. This would have much in  
446 common with the vorticity anomalies in the Tibetan Plateau anticyclone, which Hsu and Plumb  
447 (2000) found were confined to the upper troposphere. Finally, we will also note that TRMM  
448 surface precipitation may be biased across high desert landscapes like those of the NAM region,  
449 so our results should be interpreted accordingly (Huffman et al., 2007).

450         One of the conclusions from the NAME was that TUTTs act to enhance precipitation on  
451 their southeastern side *and* on their northwestern side (Finch & Johnson, 2010; Newman &

452 Johnson, 2012; Pytlak et al., 2005). Figure 10 does contain positive precipitation anomalies  
453 northwest of the TUTT center, but these did not pass the screen for statistical significance.  
454 Figure 11 shows the 95<sup>th</sup> percentile of anomalous TRMM precipitation calculated for a 5° wide  
455 band starting in the southeastern corner of our composite domain and proceeding past the TUTT  
456 center to the northwestern corner. The black line shows the result for all years. The figure  
457 implies the same result as above; precipitation is enhanced southeast of TUTTs, with the most  
458 extreme rainfall occurring more than 500 km southeast of the TUTT center. Underlain on Fig.  
459 11 are similarly constructed composites for each TRMM year. These are largely similar to each  
460 other and the mean except for the dashed burgundy line which shows an enhancement of  
461 precipitation of about 1 mm hr<sup>-1</sup> on the northwestern side of TUTTs during the NAME year  
462 (2004). We included this figure to further our assertion that our automated tracking of TUTTs is  
463 consistent with those done by hand, but it also raises the interesting question (or perhaps specter)  
464 of whether TUTTs were somehow characteristically different during the NAME year. Does the  
465 assimilation of NAME data from an otherwise sparsely observed region of North America in the  
466 ERA5 reanalysis impact that dataset's upper-tropospheric flow field, allowing ERA5 to better  
467 represent TUTTs in 2004 than in all other years? We will leave this question unanswered but  
468 provide one thought. The proposed mechanism for the enhancement of precipitation in the  
469 northwest quadrant of TUTT 4 in Newman and Johnson (2012) relies explicitly on  
470 topographically aided lifting. TUTTs may have tracked preferentially in 2004 such that small  
471 scale topographic features could help generate lift at the leading edge of TUTTs. This is  
472 speculative, as we notice nothing extraordinary about their tracks at the large scale (not shown).  
473 Finally, we will also note that we reconstructed Fig. 11 using ERA5 precipitation to the same  
474 result (not shown).

## 475 **5. Summary and Conclusions**

476           The goal of this paper was to identify and track TUTTs in time and space in a high-  
477 resolution, high-quality dataset and to better understand the relationship of TUTTs with  
478 precipitation. We used TempestExtremes to track upper-level circulation centers in the ERA5  
479 reanalysis from 1979 to 2018. Our criteria resulted in 340 long-lived TUTTs over the NAM  
480 region, which proved enough to paint a composite picture of these features.

481           We found that TUTTs exist primarily as upper-tropospheric features that, based on case  
482 studies, seem to originate from midlatitude wave breaking to the east of the NAM. TUTTs  
483 exhibit high-PV, dry air and travel westward within the mean easterly upper-level flow. Our  
484 most notable finding is that precipitation is not systematically enhanced within the main  
485 rotational flow of the TUTT. Specifically, we found no detectable increase in precipitation on  
486 the western or northwestern sides of TUTTs in the composite mean. This result contrasts with  
487 previous arguments, which relied heavily on case studies during the NAME year, that  
488 precipitation is enhanced on the western side of TUTTs due to modulations of CAPE and layer  
489 shear that enhance MCS formation (e.g. Finch and Johnson 2010, Newman and Johnson 2012).  
490 Our analysis confirms that precipitation was enhanced northwest of TUTTs during the NAME  
491 year (Fig. 11), but that year was an outlier in the combined TRMM and ERA5 datasets on which  
492 our analysis was based. This could indicate that TUTT tracks were unusual in the NAME year,  
493 consistent with the anomalously short monsoon season and poorly developed subtropical high  
494 during that year (e.g. Douglas and Englehart, 2007), or that the ERA5 reanalysis has deficiencies  
495 in its representation of TUTTs outside the NAME year. Because our conclusions regarding  
496 precipitation contrast starkly with those of previous studies, we again want to point out that  
497 TRMM 3B42 is an imperfect tool for assessing surface precipitation over the high desert but that

498 its use in this study was necessitated by our need for a long data record. Future studies might be  
499 better served by employing a more modern tool (e.g. the GPM period of IMERG or GSMaP)  
500 when any has a long enough, homogenous data record. We also found that the quasi-geostrophic  
501 ascent in the southeastern quadrant of the TUTT does not enhance precipitation and seems to be  
502 confined to the upper troposphere. Although other studies previously examined QG ascent in  
503 transient disturbances in the NAM region (e.g. Seastrand et al. 2015), our results provide the first  
504 analysis of QG vertical motion in a large ensemble of upper-tropospheric vorticity anomalies.

505 Our study has focused on the mean properties of TUTTs at the expense of deeper  
506 understanding of individual events within our dataset. An obvious omission, then, is that we  
507 have not utilized the time-space evolution data to its fullest extent. We see two opportunities in  
508 this regard for future studies. 1) We examined Rossby Wave breaking and TUTT genesis for  
509 NAME year TUTTs only. Automating that examination by pairing our data to a wave breaking  
510 database (e.g. Abatzoglou & Magnusdottir, 2006) would show statistically how frequently  
511 TUTTs are associated with summer-time wave breaking and *vice versa*. 2) Many previous  
512 investigations of TUTTs have focused on their (potentially) transient interaction with other  
513 meteorological or topographic features which may significantly, though temporarily, alter their  
514 impacts. Given the episodic nature of precipitation, it's possible that our composite view misses  
515 some interesting TUTT behavior. Employing evolutionary prototype methods (e.g. Igel 2018)  
516 might help to categorize and identify frequent development patterns of precipitation throughout  
517 the lifetime of TUTTs that are difficult to recognize from composites.

## 518 **6. Appendix**

519 The TempestExtremes v2.0 feature identification command is: `DetectNodes --`  
520 `in_data_list Inputfile --out Outputfile --searchbymin`



521 "streamfunction" --minlat 15 --maxlat 40 --minlon -120 --maxlon  
522 -90 -noclosedcontourcmd "Z,325.,4.0,1.0" --mergedist 5.0 . The  
523 command to stitch identified features in time is: StitchNodes --in Outputfile --  
524 out StitchOutputfile --maxgap 1 --minlength 67 --range 5.0.

## 525 **Acknowledgements**

526 This material is based upon work supported by the U.S. Department of Energy, Office of  
527 Science, Office of Biological and Environmental Research, Climate and Environmental Sciences  
528 Division, Regional and Global Model Analysis Program, under Award DE-SC0019367. It used  
529 resources of the National Energy Research Scientific Computing Center (NERSC), which is a  
530 DOE Office of Science User Facility. Special thanks to M. Diaz for help and D. Shaevitz for  
531 providing the QG  $\omega$  inversion code.

532

## 533 **Data Availability Statement**

534 ERA5 data are available at  
535 <https://cds.climate.copernicus.eu/#!/search?text=ERA5&type=dataset>. TRMM data are available  
536 <https://gpm.nasa.gov/data-access/downloads/trmm>. The TempestExtremes source code is  
537 available at <https://github.com/ClimateGlobalChange/tempestextremes>. The new TUTT dataset  
538 is available at <https://doi.org/10.25338/B8VS7T>.

539

540 **References**

- 541 Abatzoglou, J. T., & Magnusdottir, G. (2006). Planetary Wave Breaking and Nonlinear  
542 Reflection: Seasonal Cycle and Interannual Variability. *Journal of Climate*, 19(23), 6139–  
543 6152. <https://doi.org/10.1175/JCLI3968.1>
- 544 Adams, D. K., & Comrie, A. C. (1997). The North American Monsoon. *Bulletin of the American*  
545 *Meteorological Society*, 78(10), 2197–2213. [https://doi.org/10.1175/1520-](https://doi.org/10.1175/1520-0477(1997)078<2197:TNAM>2.0.CO;2)  
546 [0477\(1997\)078<2197:TNAM>2.0.CO;2](https://doi.org/10.1175/1520-0477(1997)078<2197:TNAM>2.0.CO;2)
- 547 Bieda, S. W., Castro, C. L., Mullen, S. L., Comrie, A. C., & Pytlak, E. (2009). The relationship  
548 of transient upper-level troughs to variability of the North American monsoon system.  
549 *Journal of Climate*, 22(15), 4213–4227. <https://doi.org/10.1175/2009JCLI2487.1>
- 550 Boos, W. R., Hurley, J. V., & Murthy, V. S. (2015). Adiabatic westward drift of Indian monsoon  
551 depressions. *Quarterly Journal of the Royal Meteorological Society*, 141(689), 1035–1048.  
552 <https://doi.org/10.1002/qj.2454>
- 553 Bosart, L., Melino, T. J., Sukup, S. R., Pytlak, E. S., E., M. J., Weiss, S. J., et al. (2011).  
554 Potential vorticity disturbances as a trigger of southwest U.S. severe weather. In *24th*  
555 *Conference on Weather and Forecasting/20th Conference on Numerical Weather*  
556 *Prediction*.
- 557 Douglas, A. V., & Englehart, P. J. (2007a). A climatological Perspective of transient synoptic  
558 features during NAME 2004. *Journal of Climate*, 20(9), 1947–1954.  
559 <https://doi.org/10.1175/JCLI4095.1>
- 560 Douglas, A. V., & Englehart, P. J. (2007b). A Climatological Perspective of Transient Synoptic

561 Features during NAME 2004. *Journal of Climate*, 20(9), 1947–1954.  
562 <https://doi.org/10.1175/JCLI4095.1>

563 Finch, Z. O., & Johnson, R. H. (2010). Observational analysis of an upper-level inverted trough  
564 during the 2004 north american monsoon experiment. *Monthly Weather Review*, 138(9),  
565 3540–3555. <https://doi.org/10.1175/2010MWR3369.1>

566 Haynes, P. H., & McIntyre, M. E. (1987). On the Representation of Rossby Wave Critical Layers  
567 and Wave Breaking in Zonally Truncated Models. *Journal of the Atmospheric Sciences*,  
568 44(17), 2359–2382. [https://doi.org/10.1175/1520-  
569 0469\(1987\)044<2359:OTRORW>2.0.CO;2](https://doi.org/10.1175/1520-0469(1987)044<2359:OTRORW>2.0.CO;2)

570 Hersbach, H., Bell, B., Berrisford, P., Hirahara, S., Horányi, A., Muñoz-Sabater, J., et al. (2020).  
571 The ERA5 Global Reanalysis. *Quarterly Journal of the Royal Meteorological Society*,  
572 qj.3803. <https://doi.org/10.1002/qj.3803>

573 Higgins, W., Ahijevych, D., Amador, J., Barros, A., Berbery, E. H., Caetano, E., et al. (2006).  
574 The NAME 2004 Field Campaign and Modeling Strategy. *Bulletin of the American  
575 Meteorological Society*, 87(1), 79–94. <https://doi.org/10.1175/BAMS-87-1-79>

576 Homeyer, C. R., & Bowman, K. P. (2013). Rossby Wave Breaking and Transport between the  
577 Tropics and Extratropics above the Subtropical Jet. *Journal of the Atmospheric Sciences*,  
578 70(2), 607–626. <https://doi.org/10.1175/JAS-D-12-0198.1>

579 Hsu, C. J., & Plumb, R. A. (2000). Nonaxisymmetric Thermally Driven Circulations and Upper-  
580 Tropospheric Monsoon Dynamics. *Journal of the Atmospheric Sciences*, 57(9), 1255–1276.  
581 [https://doi.org/10.1175/1520-0469\(2000\)057<1255:NTDCAU>2.0.CO;2](https://doi.org/10.1175/1520-0469(2000)057<1255:NTDCAU>2.0.CO;2)

582 Huffman, G. J., Bolvin, D. T., Nelkin, E. J., Wolff, D. B., Adler, R. F., Gu, G., et al. (2007). The  
583 TRMM Multisatellite Precipitation Analysis (TMPA): Quasi-Global, Multiyear, Combined-  
584 Sensor Precipitation Estimates at Fine Scales. *Journal of Hydrometeorology*, 8(1), 38–55.  
585 <https://doi.org/10.1175/JHM560.1>

586 Igel, M. R. (2018). Lagrangian Cloud Tracking and the Precipitation-Column Humidity  
587 Relationship. *Atmosphere*, 9, 289. <https://doi.org/10.3390/atmos9080289>

588 Johnson, R. H., Ciesielski, P. E., McNoldy, B. D., Rogers, P. J., & Taft, R. K. (2007). Multiscale  
589 Variability of the Flow during the North American Monsoon Experiment. *Journal of*  
590 *Climate*, 20(9), 1628–1648. <https://doi.org/10.1175/JCLI4087.1>

591 Kalnay, E., Kanamitsu, M., Kistler, R., Collins, W., Deaven, D., Gandin, L., et al. (1996). The  
592 NCEP/NCAR 40-Year Reanalysis Project. *Bulletin of the American Meteorological Society*,  
593 77(3), 437–471. [https://doi.org/10.1175/1520-0477\(1996\)077<0437:TNYRP>2.0.CO;2](https://doi.org/10.1175/1520-0477(1996)077<0437:TNYRP>2.0.CO;2)

594 Kelley, W. E., & Mock, D. R. (1982). A diagnostic study of upper tropospheric cold lows over  
595 the western North Pacific (Guam, Midway, Johnston, Wake). *Monthly Weather Review*.  
596 [https://doi.org/10.1175/1520-0493\(1982\)110<0471:ADSOUT>2.0.CO;2](https://doi.org/10.1175/1520-0493(1982)110<0471:ADSOUT>2.0.CO;2)

597 Kelly, W. E., & Mock, D. R. (1982). A Diagnostic Study of Upper Tropospheric Cold Lows  
598 Over the Western North Pacific. *Monthly Weather Review*, 110(6), 471–480.  
599 [https://doi.org/10.1175/1520-0493\(1982\)110<0471:ADSOUT>2.0.CO;2](https://doi.org/10.1175/1520-0493(1982)110<0471:ADSOUT>2.0.CO;2)

600 Krishnamurti, T. N., & Bhalme, H. N. (1976). Oscillations of a Monsoon System. Part I.  
601 Observational Aspects. *Journal of the Atmospheric Sciences*, 33(10), 1937–1954.  
602 [https://doi.org/10.1175/1520-0469\(1976\)033<1937:OOAMSP>2.0.CO;2](https://doi.org/10.1175/1520-0469(1976)033<1937:OOAMSP>2.0.CO;2)

603 Lahmers, T. M., Castro, C. L., Adams, D. K., Serra, Y. L., Brost, J. J., & Luong, T. (2016).  
604 Long-term changes in the climatology of transient inverted troughs over the North  
605 American monsoon region and their effects on precipitation. *Journal of Climate*, 29(17),  
606 6037–6064. <https://doi.org/10.1175/JCLI-D-15-0726.1>

607 Luong, T. M., Castro, C. L., Chang, H. I., Lahmers, T., Adams, D. K., & Ochoa-Moya, C. A.  
608 (2017). The more extreme nature of North American Monsoon precipitation in the  
609 Southwestern United States as revealed by a historical climatology of simulated severe  
610 weather events. *Journal of Applied Meteorology and Climatology*, 56(9), 2509–2529.  
611 <https://doi.org/10.1175/JAMC-D-16-0358.1>

612 Murthy, V. S., & Boos, W. R. (2019). Quasigeostrophic Controls on Precipitating Ascent in  
613 Monsoon Depressions. *Journal of the Atmospheric Sciences*, 77(4), 1213–1232.  
614 <https://doi.org/10.1175/JAS-D-19-0202.1>

615 Newman, A., & Johnson, R. H. (2012). Mechanisms for precipitation enhancement in a North  
616 American Monsoon upper-tropospheric trough. *Journal of the Atmospheric Sciences*, 69(6),  
617 1775–1792. <https://doi.org/10.1175/JAS-D-11-0223.1>

618 Ortega, S., Webster, P. J., Toma, V., & Chang, H. R. (2017). Quasi-biweekly oscillations of the  
619 South Asian monsoon and its co-evolution in the upper and lower troposphere. *Climate*  
620 *Dynamics*, 49(9–10), 3159–3174. <https://doi.org/10.1007/s00382-016-3503-y>

621 Papin, P. P., Bosart, L. F., & Torn, R. D. (2020). A Feature Based Approach to Classifying  
622 Summertime Potential Vorticity Streamers Linked to RossbyWave Breaking in the North  
623 Atlantic Basin. *Journal of Climate*, 5953–5969. <https://doi.org/10.1175/jcli-d-19-0812.1>

624 Prein, A. F., Langhans, W., Fosser, G., Ferrone, A., Ban, N., Goergen, K., et al. (2015). A review

625 on regional convection-permitting climate modeling: Demonstrations, prospects, and  
626 challenges. *Reviews of Geophysics*, 53(2), 323–361. <https://doi.org/10.1002/2014RG000475>

627 Pytlak, E., Goering, M., & Bennett, A. (2005). Upper tropospheric troughs and their interaction  
628 with the North American Monsoon. *85th AMS Annual Meeting, American Meteorological  
629 Society - Combined Preprints*, (1992), 281–285.

630 Rogers, P. J., & Johnson, R. H. (2007). Analysis of the 13–14 July Gulf Surge Event during the  
631 2004 North American Monsoon Experiment. *Monthly Weather Review*, 135(9), 3098–3117.  
632 <https://doi.org/10.1175/MWR3450.1>

633 Seastrand, S., Serra, Y., Castro, C., & Ritchie, E. (2015). The dominant synoptic-scale modes of  
634 North American monsoon precipitation. *International Journal of Climatology*, 35(8), 2019–  
635 2032. <https://doi.org/10.1002/joc.4104>

636 Sierks, M. D., Kalansky, J., Cannon, F., & Ralph, F. M. (2020). Characteristics, origins, and  
637 impacts of summertime extreme precipitation in the Lake Mead watershed. *Journal of  
638 Climate*, 33(7), 2663–2680. <https://doi.org/10.1175/JCLI-D-19-0387.1>

639 Ullrich, P. A., & Zarzycki, C. M. (2017). TempestExtremes: A framework for scale-insensitive  
640 pointwise feature tracking on unstructured grids. *Geoscientific Model Development*, 10(3),  
641 1069–1090. <https://doi.org/10.5194/gmd-10-1069-2017>

642 Ullrich, P. A., Zarzycki, C. M., McClenny, E. E., Pinheiro, M. C., Stanfield, A. M., & Reed, K.  
643 A. (2021). TempestExtremes v2.1: A Community Framework for Feature Detection,  
644 Tracking and Analysis in Large Datasets. *Geoscientific Model Development Discussion*.  
645 <https://doi.org/10.5194/gmd-2020-303>

646 Whitfield, M. B., & Lyons, S. W. (1992). An Upper-Tropospheric Low over Texas during  
647 Summer. *Weather and Forecasting*, 7(1), 89–106. [https://doi.org/10.1175/1520-](https://doi.org/10.1175/1520-0434(1992)007<0089:AUTLOT>2.0.CO;2)  
648 0434(1992)007<0089:AUTLOT>2.0.CO;2

649 Zarzycki, C. M., & Ullrich, P. A. (2017). Assessing sensitivities in algorithmic detection of  
650 tropical cyclones in climate data. *Geophysical Research Letters*, 44(2), 1141–1149.  
651 <https://doi.org/10.1002/2016GL071606>

652

653 **Tables**

654 **Table 1:** Comparison TUTTs identified with Tempest Extremes and subjectively in Pytlak et al.  
 655 (2005) and Sierks et al. (2020). For NAME year storms, a subjective assessment of whether the  
 656 identified TUTT is generated by midlatitude wave breaking (as determined from Fig. 3 and  
 657 Supporting figures) is included.

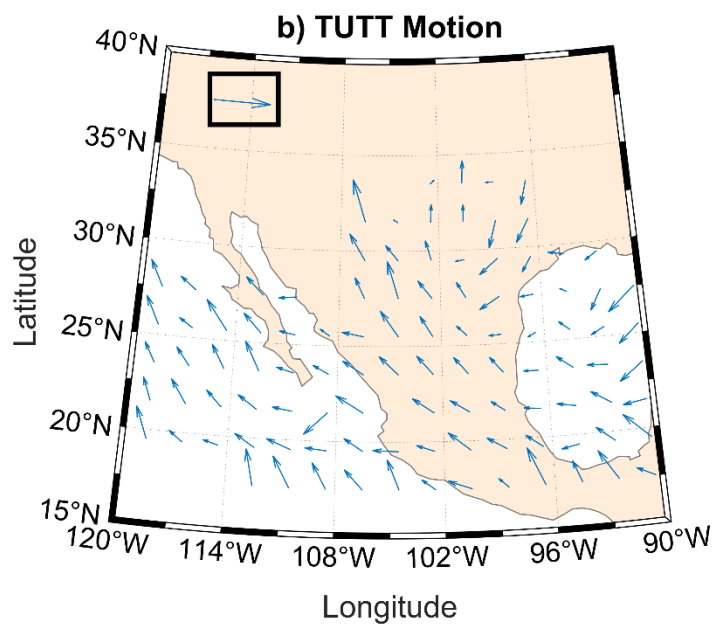
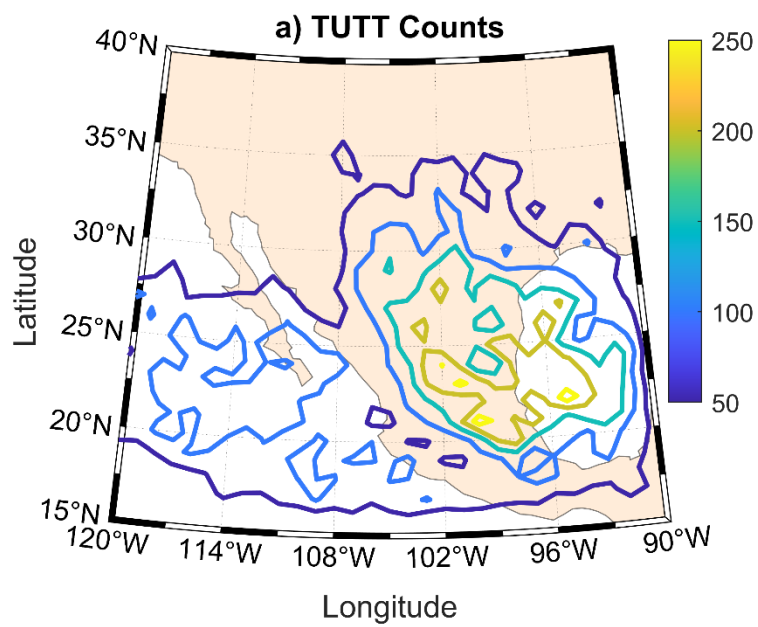
TUTT	Pytlak et al.	Tempest Extremes (Breaking?)	Permissive 0.75/1.75
3	7/5-7/10	7/3-7/6 (yes)	✓/✓
4	7/8-7/13	7/8-7/14 (yes)	✓/✓
5	7/15-7/18		✓/7/17-7/18
6	7/20-7/25	7/20-7/24 (yes)	✓/3 TUTTs
7a/b	7/29-8/2	7/29-8/1 (maybe)	✓/7/29-8/1
8	8/2-8/4		✓/x
9	8/7-8/10		✓/x
10	8/7-8/12		✓/x
$\alpha$ & Others		TUTT $\alpha$ : 7/24-7/27 (well to the east)	23/5

658

Inverted Trough/TUTT	Sierks et al	Tempest Extremes
A	8/24/1982	8/24-8/27
B	7/25/1983	7/22-7/25
C	7/22/1986	7/19-7/22
D	7/23/1998	7/20-7/27
E	7/9/1999	
F	8/30/2000	
G	7/27/2013	7/26-8/3
H	8/4/2014	

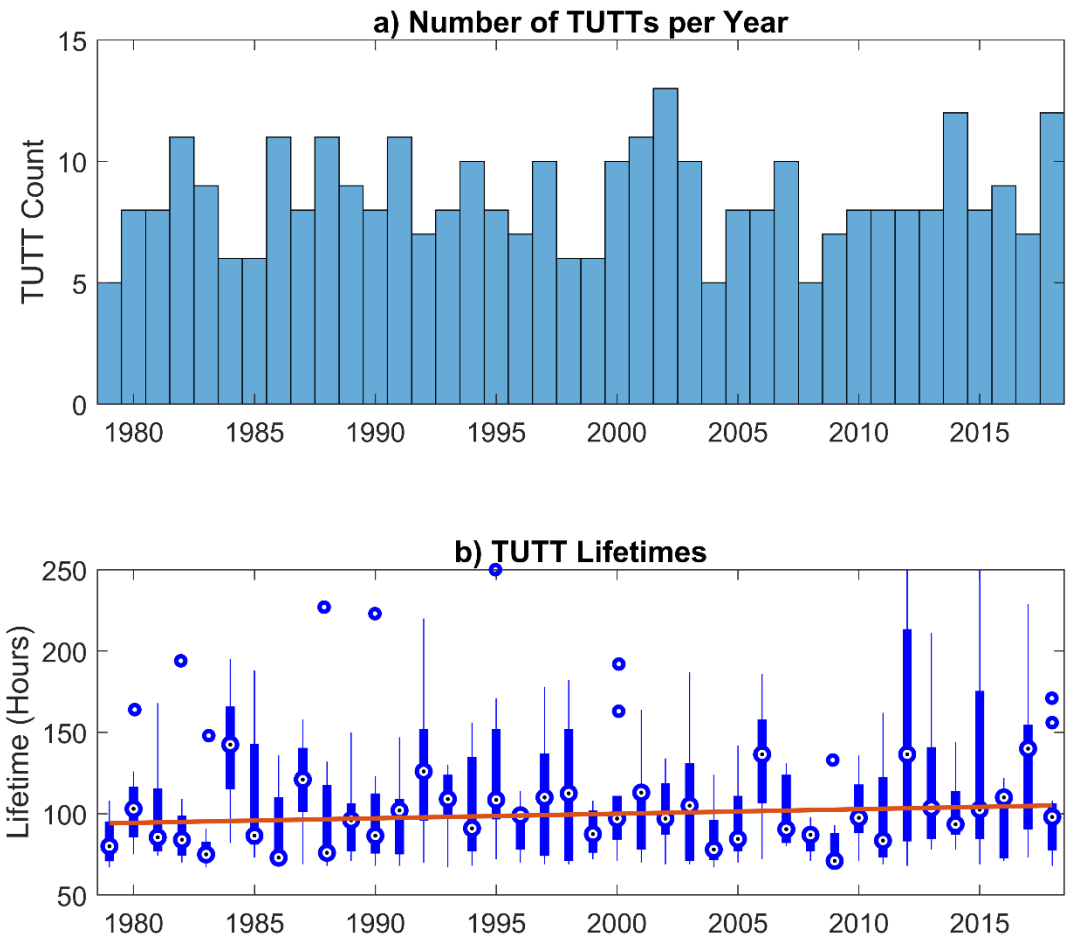
659





662 **Figure 1:** a) Total number of TUTT-center counts in  $0.25^\circ$  grid boxes. b) Mean TUTT-center  
663 velocity vectors in  $0.50^\circ$  grid boxes for such boxes with at least 50 TUTT centers. The scale of  
664 the arrow inside the black box is  $5 \text{ m s}^{-1}$ .

665

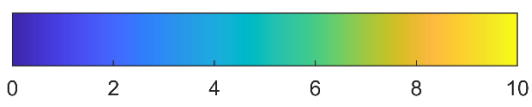
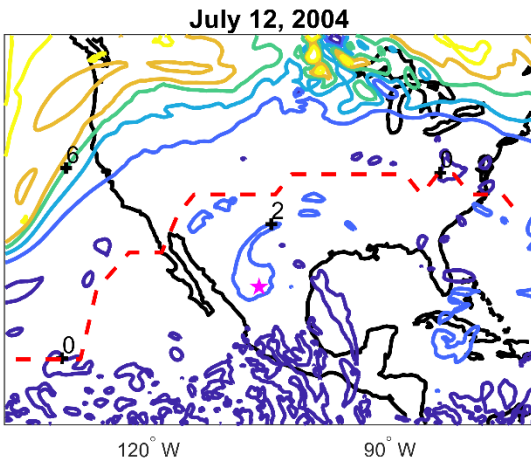
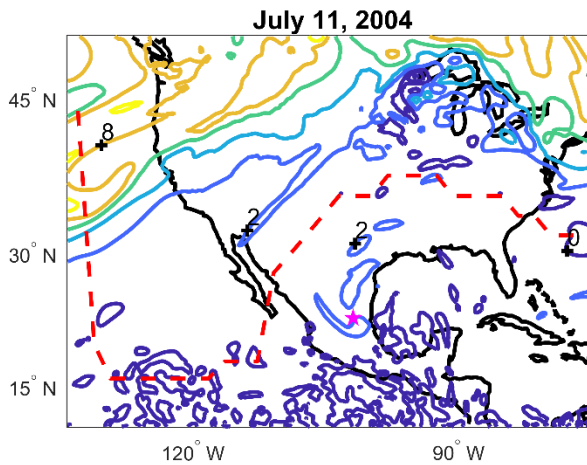
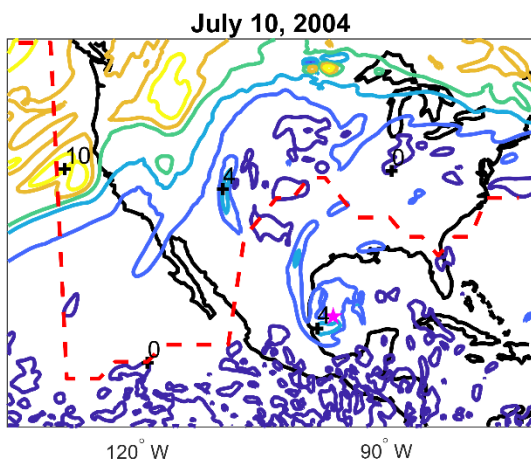
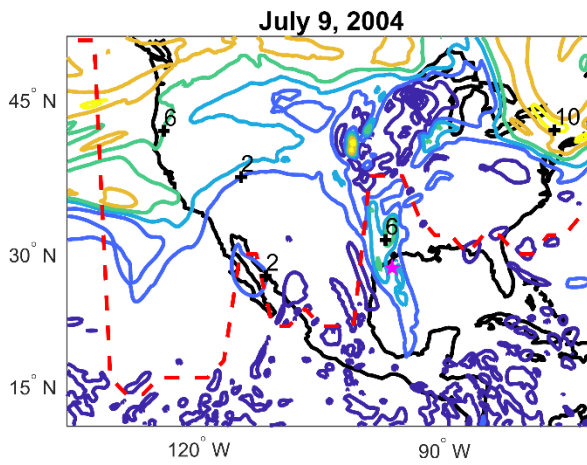
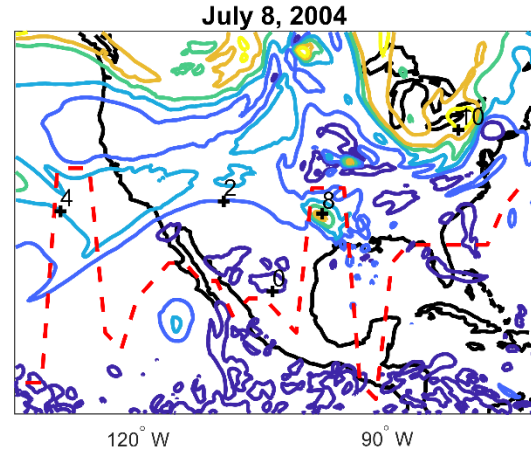
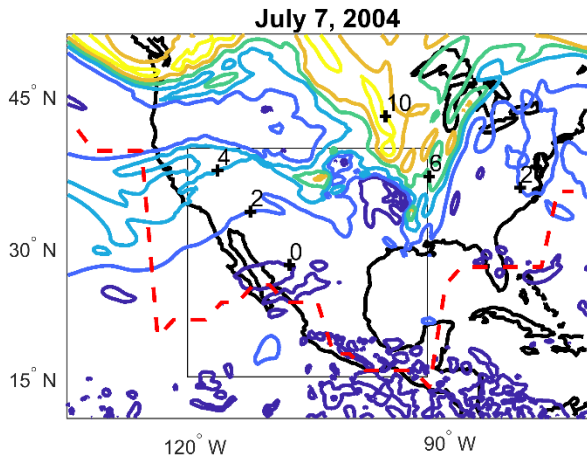


667

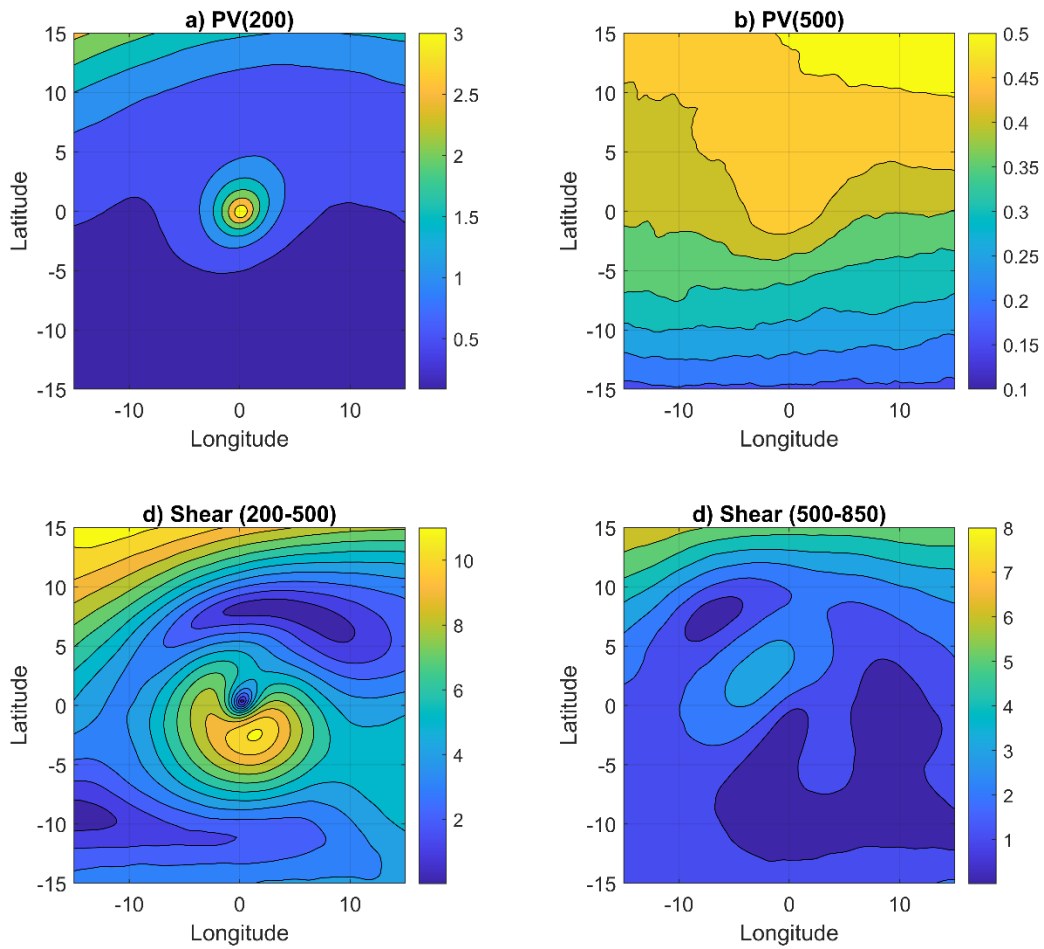
668 **Figure 2:** a) A bar plot of TUTT counts per year. b) Box and whisker plots of TUTT lifetimes

669 per year. The red line is a best fit to the data of TUTT lifetimes to the year.

670



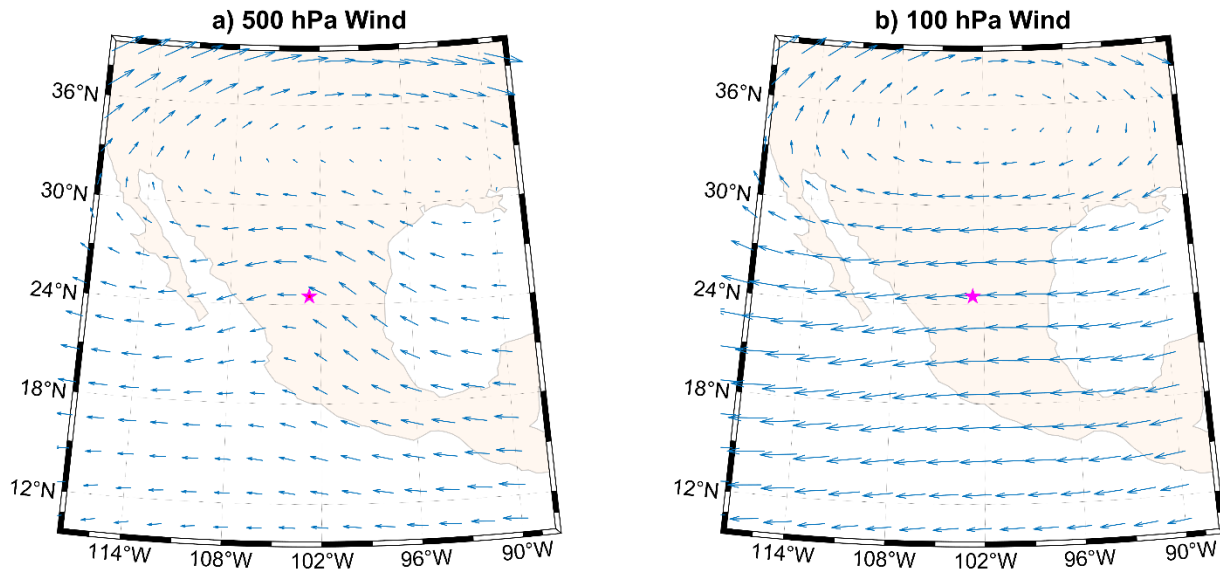
672 **Figure 3:** Maps of PV (color contours every 2 PVU with zero and negative values dark blue).  
673 PV contours are labeled intermittently near points of interest in figures for convenience. The red  
674 dashed line indicates the northernmost switch in the plotted domain from westerlies to easterlies.  
675 The pink star indicates the location of a TempestExtremes identified TUTT center. The black  
676 box included on July 7<sup>th</sup> marks the TUTT search domain.  
677



678

679 **Figure 4:** The top row shows composite mean PV at a) 200 hPa with contours spaced ever 0.5  
 680 PVU and b) at 500 hPa spaced every 0.05 PVU. The bottom row shows the magnitude of the  
 681 vertical shear of the composite mean horizontal wind with contours spaced every 1 m s<sup>-1</sup> between  
 682 c) 200 hPa and 500 hPa and d) 500 hPa and 850 hPa.

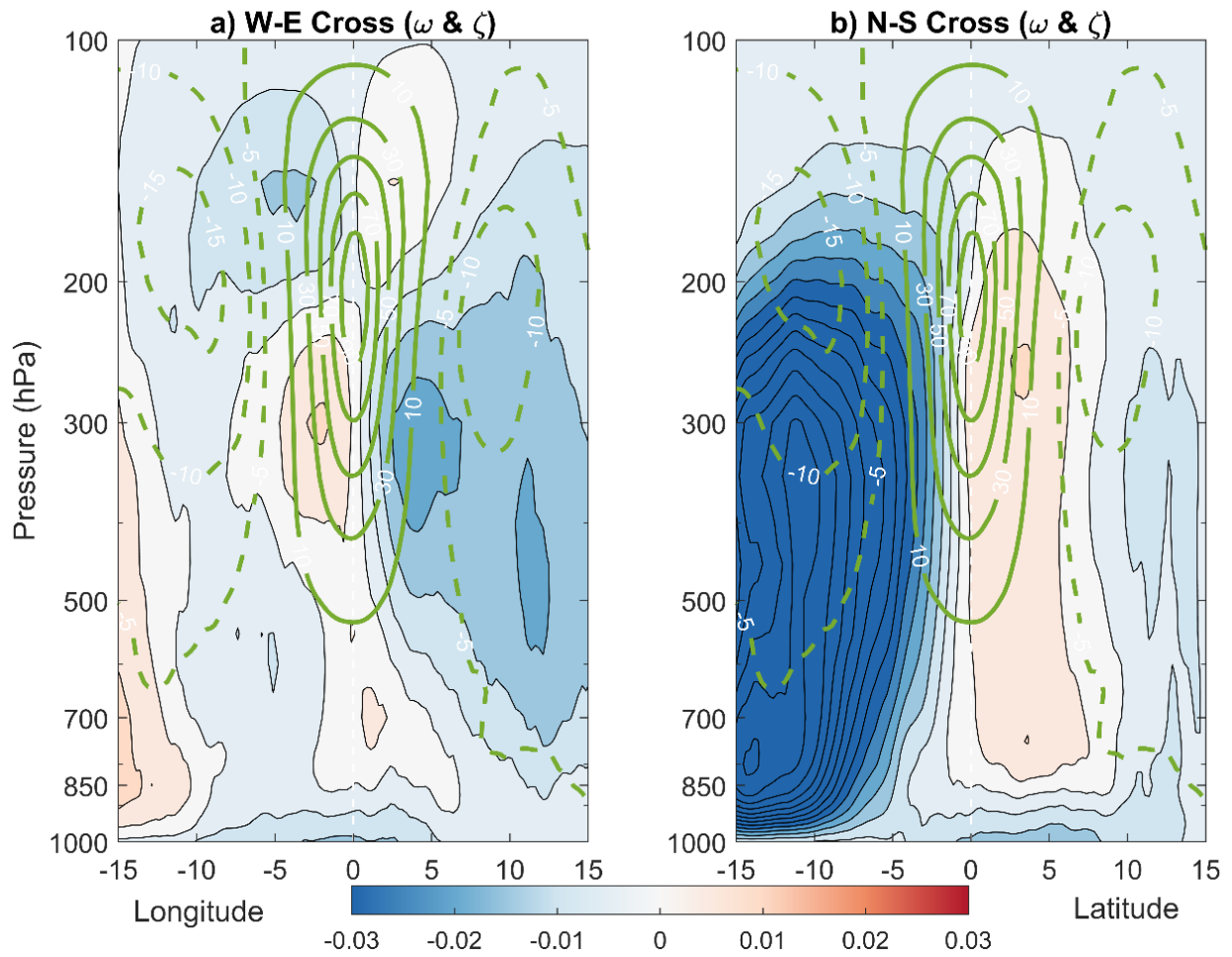
683



684

685 **Figure 5:** Wind vectors for the mean a) 500 hPa and b) 100 hPa flow. Composite mean flow is  
 686 projected on a map centered on the mean TUTT center location for context which is marked with  
 687 a red star. Wind vectors are plotted every 2°. The maximum magnitude of a wind barb in both  
 688 a) and in b) is 10 m s<sup>-1</sup>.

689



690

691 **Figure 6:** Composite mean cross sections of anomalous pressure velocity in colored shading and

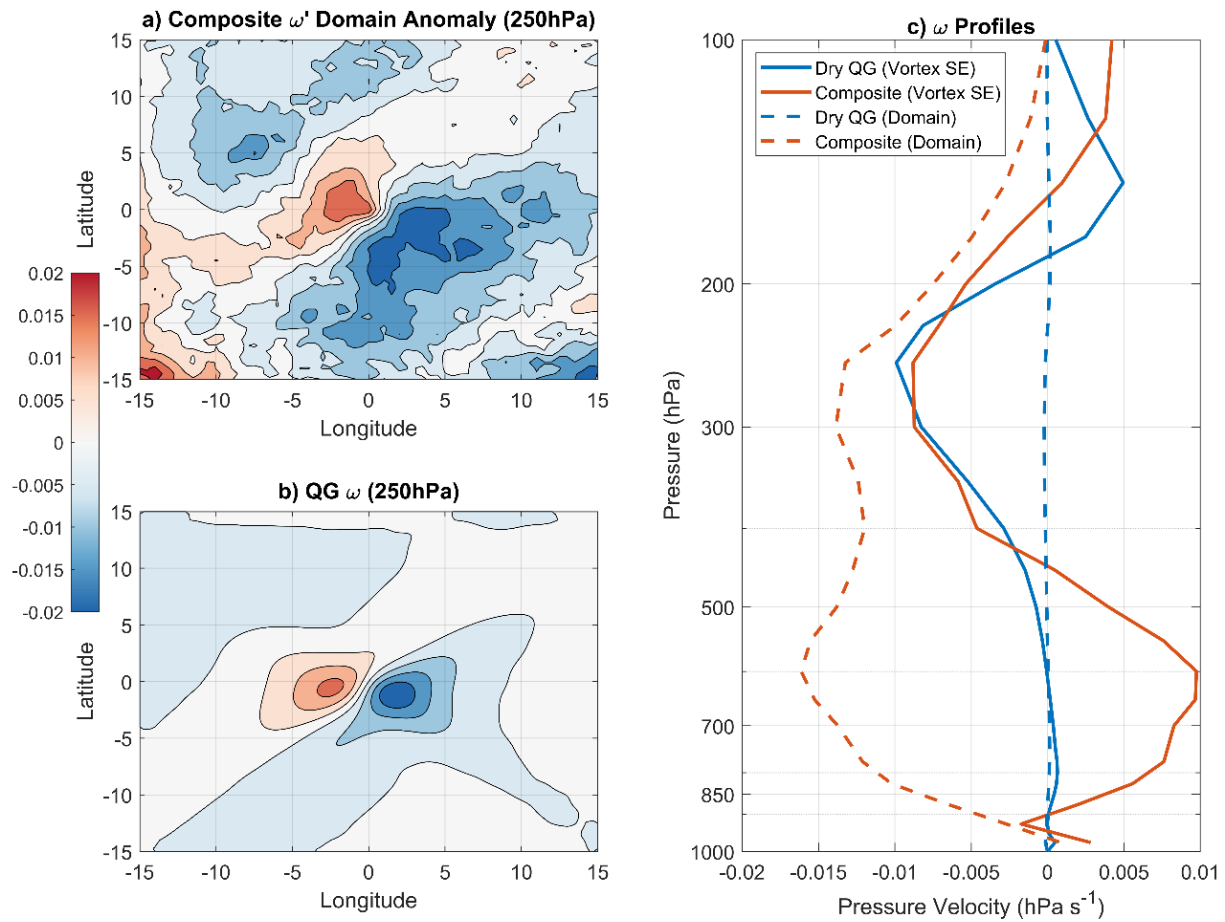
692 relative vorticity in green contours with white labels. a) A zonal cross section averaged within

693  $5^\circ$  latitude of the composite center. b) A meridional cross section averaged within  $5^\circ$  longitude of

694 the composite center.

695





696

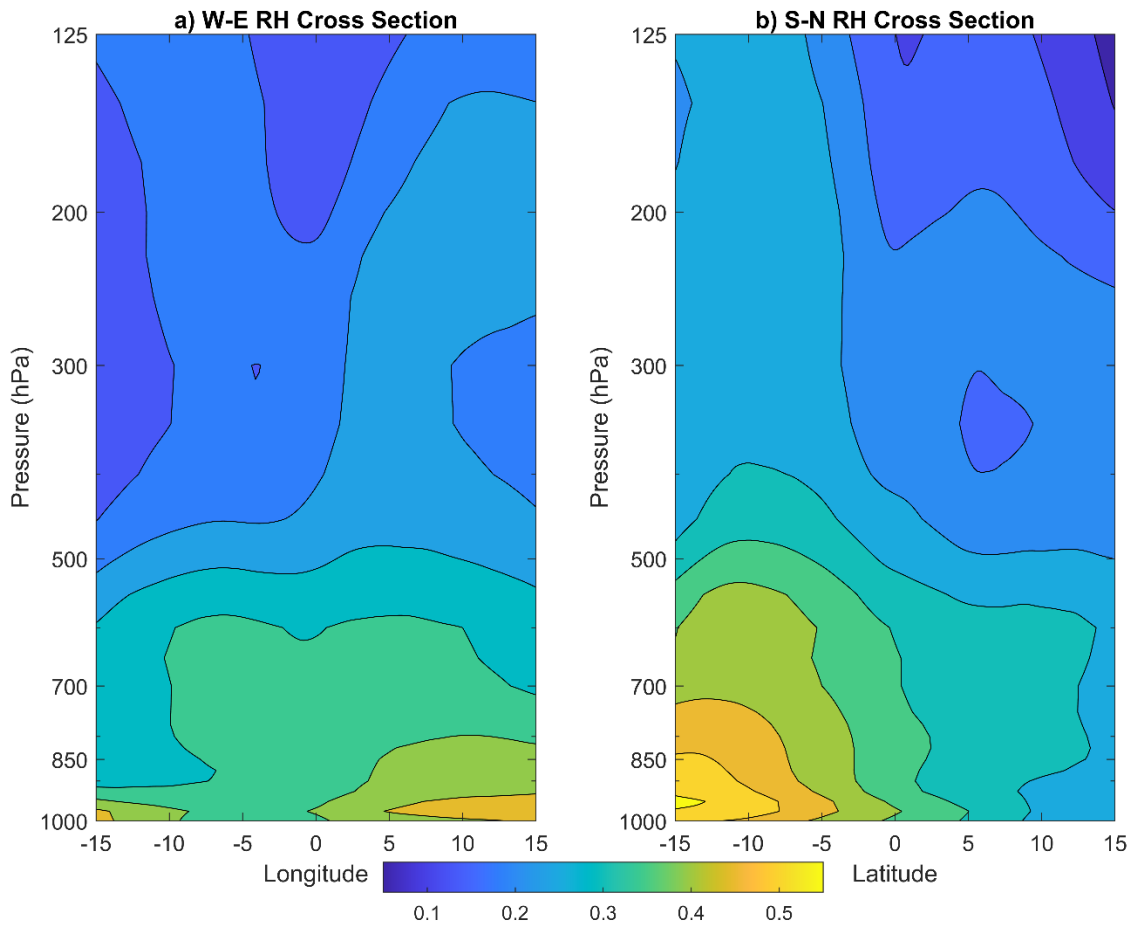
697 **Figure 7:** Comparisons between the anomaly of composite  $\omega$  and that derived from the QG

698 inversion. a) Map of the anomaly of composite  $\omega$  at 250 hPa. b) Map of inverted QG  $\omega$ . c)

699 Vertical profiles of both  $\omega$  quantities for a  $5^\circ$  square to the southeast of the vortex composite

700 point and for the whole domain. “Dry QG” implies that we do not invert the diabatic term.

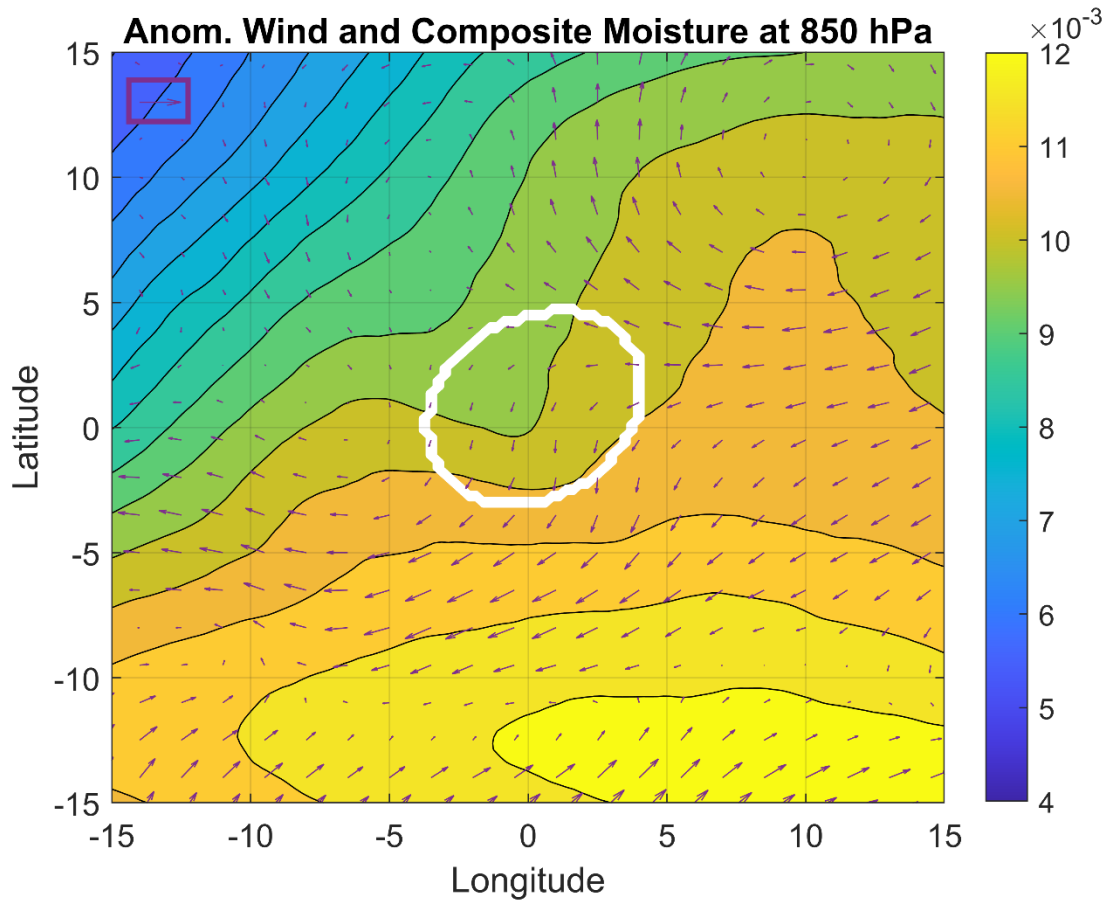
701



702

703 **Figure 8:** Like Fig. 6 except for relative humidity (not anomalous).

704

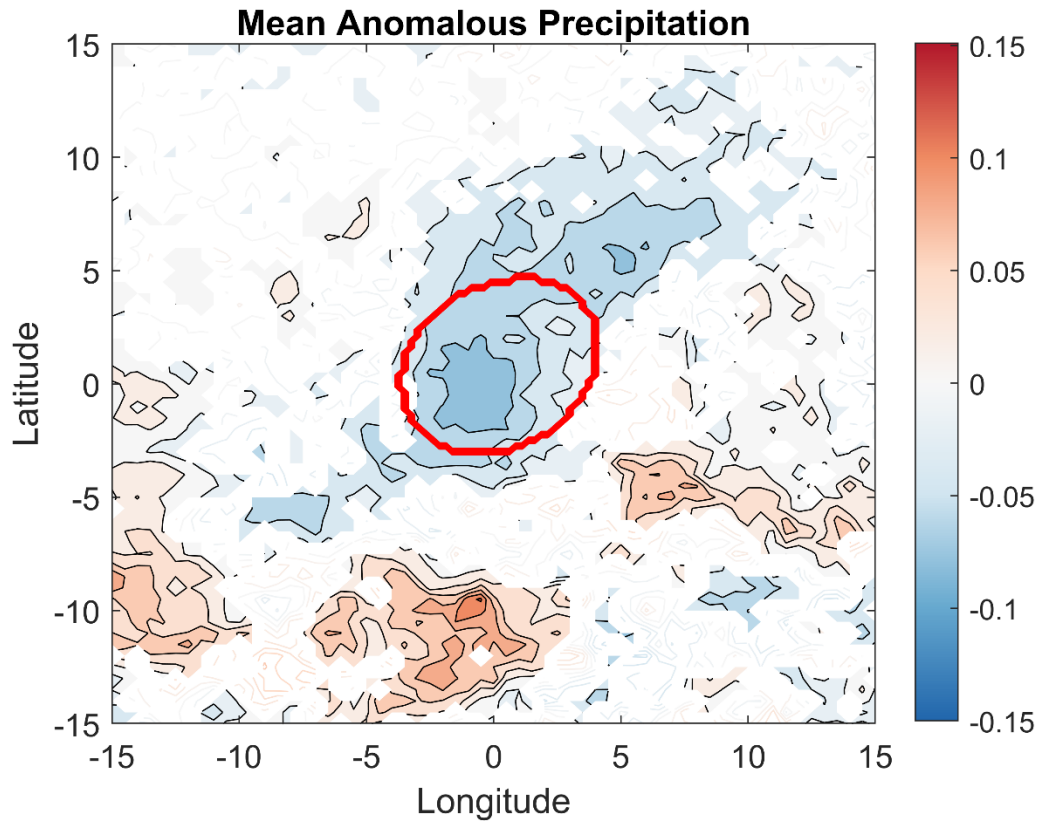


705

706 **Figure 9:** Composite mean anomalous winds (purple vectors) overlain on composite mean  
 707 moisture mixing ratio both at 850 hPa. The magnitude of the vector in the purple box is  $1 \text{ m s}^{-1}$ .

708 The white line outlines the 1 PVU contour at 200 hPa.

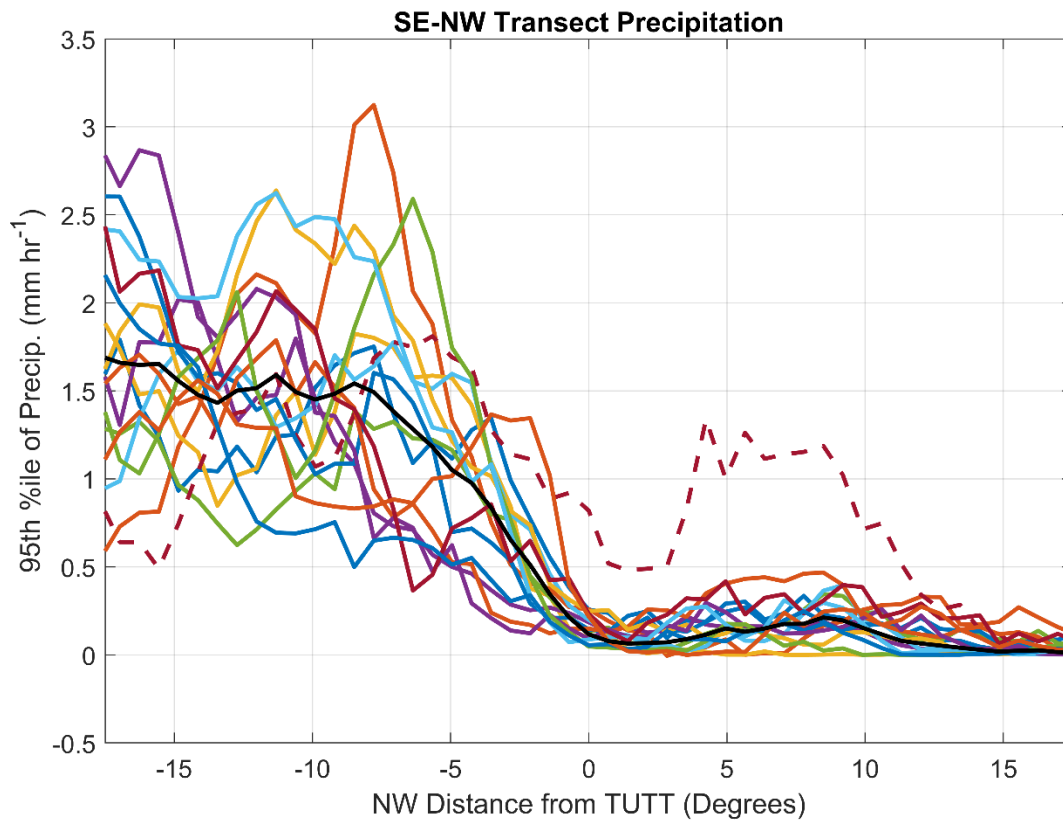
709



710

711 **Figure 10:** Spatial composites of the mean anomalous precipitation rate. Statistically significant  
 712 anomalies are shown in filled contours; not-significant values are shown in open contours. The  
 713 thick red line outlines the 1 PVU contour at 200 hPa.

714



715

716 **Figure 11:** The 95<sup>th</sup> percentile of anomalous precipitation rate for precipitation occurring within  
 717 5° of a line running diagonally from the southeast to the northwest through the composite TUTT  
 718 center. The black line is for all years. Colored lines indicate individual years. The burgundy  
 719 dashed line shows data from 2004.

720